Cite as: S. Tsesses *et al.*, *Science* 10.1126/science.aau0227 (2018).

Optical skyrmion lattice in evanescent electromagnetic fields

S. Tsesses[1], E. Ostrovsky[1], K. Cohen[1], B. Gjonaj[2], N. Lindner[3], G. Bartal[1]*

[1]Andrew and Erna Viterbi Department of Electrical Engineering, Technion–Israel Institute of Technology, 3200003 Haifa, Israel. [2]Faculty of Medical Sciences, Albanian University, Durrës Street, Tirana 1000, Albania. [3]Physics Department, Technion–Israel Institute of Technology, 3200003 Haifa, Israel.

***Corresponding author. Email: guy@ee.technion.ac.il**

Topological defects play a key role in a variety of physical systems, ranging from high-energy to solid state physics. A skyrmion is a type of topological defect that has shown promise for applications in the fields of magnetic storage and spintronics. We show that optical skyrmion lattices can be generated using evanescent electromagnetic fields and demonstrate this using surface plasmon polaritons, imaged by phase-resolved near-field optical microscopy. We show how the optical skyrmion lattice exhibits robustness to imperfections while the topological domain walls in the lattice can be continuously tuned, changing the spatial structure of the skyrmions from bubble-type to Néel-type. Extending the generation of skyrmions to photonic systems provides various possibilities for applications in optical information processing, transfer and storage.

Topological defects are field configurations which cannot be deformed to a standard, smooth shape. They are at the core of many fascinating phenomena in hydrodynamics, aerodynamics, exotic phases of matter (*1*, *2*), cosmology (*3*) and optics (*4*) and, in many cases, are of importance to practical applications. The intricate dynamics of a multitude of topological defects and the efforts to control them are of key importance in high-temperature superconductivity (*5*) and topological phase transitions such as the Berezinskii–Kosterlitz–Thouless transition (*6*).

One type of topological defect is a skyrmion (*7*), a topologically stable configuration of a three-component vector field in two dimensions. Skyrmions were initially developed theoretically in elementary particles and have since been demonstrated in Bose-Einstein condensates (*8*), nematic liquid crystals (*9*) and as a phase transition in chiral magnets (*10*, *11*). The skyrmion lattice phase and single magnetic skyrmions (*12*, *13*) are currently considered a promising route toward high-density magnetic information storage and transfer (*14*, *15*), as they are very robust to material defects and can be driven by low applied currents (*12*, *16*, *17*). A skyrmion may take on various shapes, which are all topologically equivalent. Bloch-type (*11*) and Néel-type (*18*) skyrmions exhibit a smoothly varying field configuration, with the derivatives of the vector field spread out in space. In bubble-type skyrmions (*19*, *20*), the variations of the vector field are confined to line-like areas, known as topological domain walls, which separate two domains in which the field vectors are opposite.

In optics, topological phenomena have been researched intensely in the past decade. Since the first observation of photonic topological insulators (*21*), optical topological phenomena have been rigorously studied, both theoretically and experimentally (*22*–*25*), with applications such as topologically-protected lasing (*26*–*28*). In fact, topological defects in optics were first extensively explored via phase and polarization singularities, both in free-space propagating light (*29*–*31*) and two-dimensionally confined light (*32*–*34*). However, only recently has there been any experimental investigation of optical topological domain walls (*35*), while the field of optical skyrmions has so far remained untapped.

Formation of optical skyrmion lattices

The configuration of a three component real vector field on a two dimensional space provides a smooth mapping of that space to the unit sphere. The topological invariant which identifies skyrmions counts the number of times the field configuration covers the entire sphere. This topological invariant, which we denote by S, is known as the skyrmion number and takes integer values. For the skyrmion to be topologically robust, the space on which it is defined cannot have a boundary. This condition is indeed satisfied by a periodic field configuration, in which a skyrmion is obtained in each unit cell of a lattice. For such a "skyrmion lattice" configuration, the skyrmion number can be written in an integral form:

$$S = \frac{1}{4\pi}\int_A s dA \quad (1)$$

Where the area A covers one unit cell of the lattice and $s = \vec{e}\cdot\left[\left(\partial\vec{e}/\partial x\right)\times\left(\partial\vec{e}/\partial y\right)\right]$ is the skyrmion number density; $\vec{e}$ is a real, normalized, three-component field; and x, y are

directions in the two dimensional plane. The skyrmion number S, being an integer, is robust to deformations of the field $\vec{\mathrm{e}}$ as long as $\vec{\mathrm{e}}$ remains non-singular and maintains the periodicity of the lattice.

We find that the electric field vector of electromagnetic waves can be structured so as to meet all the requirements needed to create a skyrmion lattice, similarly to the magnetization vector of the skyrmion lattices in chiral magnets. Being a three-dimensional field in a two-dimensional space, optical skyrmions must be formed by electromagnetic waves confined to two dimensions, such as in guided waves. A more thorough explanation as to why free-space electromagnetic waves do not exhibit skyrmions can be found in the Supplementary.

Consider an electric field comprised of six interfering Transverse Magnetic (TM) guided waves with equal amplitudes, freely propagating in the transverse ($x-y$) plane and evanescently decaying in the axial direction (z). The six waves are directed toward each other in the transverse plane and possess transverse wave vectors of similar magnitude, such that they create three standing waves in 0°, 60° and 120°. The axial (out-of-plane) field component in the frequency domain can therefore be expressed as a sum of three cosine functions:

$$E_z^{(\omega)} = E_0 e^{-|k_z|z} \sum_{\theta=-\frac{\pi}{3},0,\frac{\pi}{3}} \cos\left(k_{\|}\left[\cos(\theta)x+\sin(\theta)y\right]\right) \quad (2)$$

Where E_0 is a real normalization constant and $k_{\|}, k_z$ are the transverse and axial components of the wave vector ($k_{\|}$ is real and k_z is imaginary), such that $k_{\|}^2 + k_z^2 = k_0^2$ (k_0 is the free-space wavenumber). The transverse (in-plane) electric field components in the frequency domain can be readily derived from Maxwell's equations:

$$\begin{pmatrix} E_x^{(\omega)} \\ E_y^{(\omega)} \end{pmatrix} = -E_0 \frac{|k_z|}{k_{\|}} e^{-|k_z|z} \sum_{\theta=-\frac{\pi}{3},0,\frac{\pi}{3}} \begin{pmatrix} \cos(\theta) \\ \sin(\theta) \end{pmatrix} \sin\left(k_{\|}\left[\cos(\theta)x+\sin(\theta)y\right]\right) \quad (3)$$

Namely, for waves evanescently decaying in one dimension, all electric field components are entirely real (up to a global phase), allowing to define a real unit vector $\vec{\mathrm{e}} = \vec{E}/|\vec{E}|$ associated with the electric field and enabling a description of the field configuration as an optical skyrmion lattice. This is a direct consequence of the phase added in the spin-momentum locking process of evanescent electromagnetic fields (*36*) and hence does not hold for propagating waves [see (*37*), section S.1].

Figure 1 depicts the electric field described by Eqs. 2 and 3, for $|k_z| \approx |k_{\|}| > k_0$. The axial electric field has the form of a hexagonally-symmetric lattice (Fig. 1A). The transverse field follows the same symmetry, yet possesses pronounced polarization singularities, which are expressed by zero-amplitude points at the center of each lattice site (Fig. 1B), at which the field direction is ill-defined (Fig. 1C). The normalized three-dimensional electric field (Fig. 1D) confirms the formation of a skyrmion lattice – each lattice site exhibits the distinct features of a Néel-type skyrmion (*18*), with their calculated skyrmion number, using Eq. 1, being $S = 1$.

Formation of the optical skyrmion lattice can be represented in the momentum space as a transition from free-space propagation in 3D ($|k_{\|}| < k_0$) to guided mode propagation in 2D ($|k_{\|}| > k_0$). To rigorously describe this transition, we must expand the skyrmion number definition to complex electromagnetic fields, by defining $\vec{\mathbf{e}}$ in Eq. 1, as the real part of the local unit vector of the electric field. This new definition is consistent with the prior description of optical skyrmions in the ideal case, which is determined by Eqs. 2 and 3 in a lossless medium. Figure 2 presents the transition, by showing the skyrmion number in a single lattice site as a function of $k_{\|}$ using the above definition for $\vec{\mathrm{e}}$.

Figure 2 also shows the skyrmion number density contrast ($\psi = [s_{\max} + s_{\min}]/[s_{\max} - s_{\min}]$) in a single lattice site as a function of $k_{\|}$, which is a parameter providing a quantitative measure of the spatial confinement of the skyrmion density. For $k_{\|}$ slightly larger than k_0, the skyrmions are spatially confined (density contrast close to 1), with clear domain walls separating between two specific field states, effectively creating bubble-type skyrmions (point A). As $k_{\|}$ grows, the domain walls start to smear (point B), creating skyrmions with increasingly uniform skyrmion number density, converging to the Néel-type field formation shown in Fig. 1 (point C, density contrast of 0.5). This stems directly from the scaling factor $|k_z|/k_{\|}$, which can be tuned by varying the effective index (normalized propagation constant) of a guided mode.

Observation of an optical skyrmion lattice

Observing the optical skyrmion lattice has several prerequisites: First, it requires a physical system allowing two-dimensional guided waves to propagate in six specific directions, while interfering them with carefully controlled phase differences. Second, it necessitates a measurement apparatus that will enable the phase-resolved imaging of such electromagnetic waves at a resolution far better than the optical diffraction limit. Additionally, a non-ideal physical system, e.g., one that is finite and with inherent losses, provides an excellent platform to examine the robustness of the topological properties of the optical skyrmions.

Such losses distort the unit vector $\vec{\mathrm{e}} = \vec{E}/|\vec{E}|$ associated with the electric field, and create an unwanted phase difference between its components. However, in the regime of

small losses, the configuration of the real part of the field still yields a well-defined skyrmion lattice, while being sufficiently larger than the imaginary part such that the latter is negligible [see full derivation in (*37*), section S.3]. In this regime, the skyrmion number S deviates slightly from its quantized value at zero losses due to the weak breaking of the lattice translation symmetry, increasingly more so for unit cells which are farther away from the point of origin. Figure 3 gives a quantitative connection between the amount of loss and the robustness of the skyrmion number, showing the number of unit cells exhibiting $S > 0.99$. For example, a configuration in which 49 sites exhibit $S > 0.99$ is obtained if the electromagnetic waves creating it persist for roughly 400 periods before decaying – an easily achieved goal in many photonic systems.

A physical system capable of fulfilling the above-mentioned requirements are surface plasmon polaritons (SPPs) (*38*) – electromagnetic surface waves existing at the interface between metallic and dielectric materials. SPPs only exist in TM polarization and the phase difference between SPPs propagating along different directions can be easily controlled (*39*). Furthermore, they are by design an imperfect system, due to the ohmic losses generated by the metal.

In our system (see Fig. 4), SPPs are excited at the interface of air and gold, resulting in both a small propagation decay and a transverse wave vector just slightly larger than the free-space wavenumber [$k_{\parallel} = (1.038 + i0.003)k_0$]. Circularly polarized light impinges on a specially designed, hexagonally-shaped coupling slit, exciting surface plasmon polaritons from each slit edge toward its center. The slit provides the same phase to the SPPs created by all edges, yet not exactly the same amplitude (due to a different propagation length of the SPPs generated by two of the edges and their propagation loss). This results in a distortion of the skyrmion lattice, which, together with the finite structure, helps in examining its robustness.

In the experimental setup used to detect optical skyrmions [see (*37*) and fig. S1], a scattering near-field scanning optical microscope (s-NSOM) enables phase-resolved measurement of the electric field normal to the surface by means of pseudo-heterodyne interferometric detection (*40*). The ability to detect phase information is crucial, as it not only provides the full axial electric field, but also allows to perform a spatial Fourier transform (and its inverse), in order to filter out noises. The phase information, filtering ability and high spatial resolution of the measurement enable the correct extraction of the transverse field components and thus – of the skyrmion number.

The plasmonic wavenumber and applied boundary conditions create a plasmonic skyrmion lattice in the central part of the sample with characteristics typical to bubbles (Fig. 5). These characteristics are a result of the relatively small transverse wave vector, leading to an axial field component 5 times larger than the transverse ones. While the real electric field is slightly distorted, as expected (Fig. 5, A to C), it still shows similarity to the electric field configuration presented in Fig. 1. The extracted skyrmion number density at the center of the lattice (Fig. 5E) resembles that of the bubble-type skyrmion lattice shown in the inset of Fig. 2 (point A). Calculating the skyrmion number in each lattice site, we reach the result $S = 0.997 \pm 0.058$, thus demonstrating the robustness of the optical skyrmions.

Although not demonstrated experimentally in this work, the generation of a single skyrmion in the electric field of evanescent electromagnetic waves is possible as well [see (*37*), section S.5]. A single optical skyrmion may be achieved by engineering finite boundary conditions while still preserving a closed manifold, in a similar manner to schemes already suggested and observed in magnetic skyrmions (*41*, *42*).

Discussion

We show here that a skyrmion lattice can be obtained as a solution to a linear plasmonic system by proper engineering of the boundary conditions and the transverse momentum of the electro-magnetic waves. The topological invariant classifying the skyrmions in the lattice is protected by the lattice symmetry, and the lattice itself may be realized in any photonic system with evanescent waves, e.g., planar waveguide modes and waves undergoing total internal reflection (TIR).

The generation of an optical skyrmion lattice paves the way toward inducing skyrmion lattices "on-demand" in matter systems (e.g., cold atoms or dielectric particles in a fluid) through light-matter interactions. Namely, this will allow stimulated creation of skyrmions in matter, as opposed to skyrmions in all other systems [including optically-excited skyrmions in chiral magnets (*43*)], which are spontaneously created.

Furthermore, optical nonlinearity in systems supporting evanescent waves (e.g., SPPs in gold or nonlinear dielectric waveguides) could give rise to soliton-like skyrmion states exhibiting a topologically-protected skyrmion number, which will be robust against external perturbation.

In this article, we focused on TM polarized electromagnetic waves, which exhibited a skyrmion lattice in the electric field. Arranging Transverse Electric (TE) polarized waves in a similar way, using a dielectric waveguide or by TIR, would create skyrmions in the magnetic field of the electromagnetic wave, with the potential to stimulate a skyrmion lattice not only electrically, but also magnetically, using either femtosecond pulsed excitations or sub-millikelvin temperatures.

Optical skyrmion lattices could also bring about new optical effects, highlighting their potential applications in optical information processing, storage and transfer. For

example, in light emission processes such as fluorescence or harmonic generation, the unique field configuration of optical skyrmions would result in the simultaneous emission of all possible polarizations in a structured, phase-locked and coherent way. Alternatively, probe beams could nonlinearly interact with the skyrmion lattice via Kerr nonlinearity and be affected by a complex, polarization-dependent Berry curvature.

REFERENCES AND NOTES

1. J. Bardeen, M. J. Stephen, Theory of the motion of vortices in superconductors. *Phys. Rev.* **140**, A1197–A1207 (1965). doi:10.1103/PhysRev.140.A1197
2. M. R. Matthews, B. P. Anderson, P. C. Haljan, D. S. Hall, C. E. Wieman, E. A. Cornell, Vortices in a Bose-Einstein condensate. *Phys. Rev. Lett.* **83**, 2498–2501 (1999). doi:10.1103/PhysRevLett.83.2498
3. T. W. B. Kibble, Topology of cosmic domains and strings. *J. Phys. Math. Gen.* **9**, 1387–1398 (1976). doi:10.1088/0305-4470/9/8/029
4. L. Allen, M. W. Beijersbergen, R. J. C. Spreeuw, J. P. Woerdman, Orbital angular momentum of light and the transformation of Laguerre-Gaussian laser modes. *Phys. Rev. A* **45**, 8185–8189 (1992). doi:10.1103/PhysRevA.45.8185 Medline
5. G. Blatter, M. V. Feigel'man, V. B. Geshkenbein, A. I. Larkin, V. M. Vinokur, Vortices in high-temperature superconductors. *Rev. Mod. Phys.* **66**, 1125–1388 (1994). doi:10.1103/RevModPhys.66.1125
6. J. M. Kosterlitz, D. J. Thouless, Ordering, metastability and phase transitions in two-dimensional systems. *J. Phys. C Solid State Phys.* **6**, 1181–1203 (1973). doi:10.1088/0022-3719/6/7/010
7. T. H. R. Skyrme, A unified field theory of mesons and baryons. *Nucl. Phys.* **31**, 556–569 (1962). doi:10.1016/0029-5582(62)90775-7
8. U. Al Khawaja, H. Stoof, Skyrmions in a ferromagnetic Bose-Einstein condensate. *Nature* **411**, 918–920 (2001). doi:10.1038/35082010 Medline
9. J. Fukuda, S. Žumer, Quasi-two-dimensional Skyrmion lattices in a chiral nematic liquid crystal. *Nat. Commun.* **2**, 246 (2011). doi:10.1038/ncomms1250 Medline
10. S. Mühlbauer, B. Binz, F. Jonietz, C. Pfleiderer, A. Rosch, A. Neubauer, R. Georgii, P. Böni, Skyrmion lattice in a chiral magnet. *Science* **323**, 915–919 (2009). doi:10.1126/science.1166767 Medline
11. X. Z. Yu, Y. Onose, N. Kanazawa, J. H. Park, J. H. Han, Y. Matsui, N. Nagaosa, Y. Tokura, Real-space observation of a two-dimensional skyrmion crystal. *Nature* **465**, 901–904 (2010). doi:10.1038/nature09124 Medline
12. N. Romming, C. Hanneken, M. Menzel, J. E. Bickel, B. Wolter, K. von Bergmann, A. Kubetzka, R. Wiesendanger, Writing and deleting single magnetic skyrmions. *Science* **341**, 636–639 (2013). doi:10.1126/science.1240573 Medline
13. D. Maccariello, W. Legrand, N. Reyren, K. Garcia, K. Bouzehouane, S. Collin, V. Cros, A. Fert, Electrical detection of single magnetic skyrmions in metallic multilayers at room temperature. *Nat. Nanotechnol.* **13**, 233–237 (2018). doi:10.1038/s41565-017-0044-4 Medline
14. A. Fert, V. Cros, J. Sampaio, Skyrmions on the track. *Nat. Nanotechnol.* **8**, 152–156 (2013). doi:10.1038/nnano.2013.29 Medline
15. N. Nagaosa, Y. Tokura, Topological properties and dynamics of magnetic skyrmions. *Nat. Nanotechnol.* **8**, 899–911 (2013). doi:10.1038/nnano.2013.243 Medline
16. X. Z. Yu, N. Kanazawa, W. Z. Zhang, T. Nagai, T. Hara, K. Kimoto, Y. Matsui, Y. Onose, Y. Tokura, Skyrmion flow near room temperature in an ultralow current density. *Nat. Commun.* **3**, 988 (2012). doi:10.1038/ncomms1990 Medline
17. J. Sampaio, V. Cros, S. Rohart, A. Thiaville, A. Fert, Nucleation, stability and current-induced motion of isolated magnetic skyrmions in nanostructures. *Nat. Nanotechnol.* **8**, 839–844 (2013). doi:10.1038/nnano.2013.210 Medline
18. I. Kézsmárki, S. Bordács, P. Milde, E. Neuber, L. M. Eng, J. S. White, H. M. Rønnow, C. D. Dewhurst, M. Mochizuki, K. Yanai, H. Nakamura, D. Ehlers, V. Tsurkan, A. Loidl, Néel-type skyrmion lattice with confined orientation in the polar magnetic semiconductor GaV4S8. *Nat. Mater.* **14**, 1116–1122 (2015). doi:10.1038/nmat4402 Medline
19. C. Kooy, U. Enz, Experimental and theoretical study of the domain configuration in thin layers of $BaFe_{12}O_{19}$. *Philips Res. Rep.* **15**, 7–29 (1960).
20. C. Moutafis, S. Komineas, J. A. C. Bland, Dynamics and switching processes for magnetic bubbles in nanoelements. *Phys. Rev. B* **79**, 224429 (2009). doi:10.1103/PhysRevB.79.224429
21. Z. Wang, Y. Chong, J. D. Joannopoulos, M. Soljačić, Observation of unidirectional backscattering-immune topological electromagnetic states. *Nature* **461**, 772–775 (2009). doi:10.1038/nature08293 Medline
22. K. Fang, Z. Yu, S. Fan, Realizing effective magnetic field for photons by controlling the phase of dynamic modulation. *Nat. Photonics* **6**, 782–787 (2012). doi:10.1038/nphoton.2012.236
23. A. B. Khanikaev, S. H. Mousavi, W.-K. Tse, M. Kargarian, A. H. MacDonald, G. Shvets, Photonic topological insulators. *Nat. Mater.* **12**, 233–239 (2013). doi:10.1038/nmat3520 Medline
24. M. C. Rechtsman, J. M. Zeuner, Y. Plotnik, Y. Lumer, D. Podolsky, F. Dreisow, S. Nolte, M. Segev, A. Szameit, Photonic Floquet topological insulators. *Nature* **496**, 196–200 (2013). doi:10.1038/nature12066 Medline
25. M. Hafezi, S. Mittal, J. Fan, A. Migdall, J. M. Taylor, Imaging topological edge states in silicon photonics. *Nat. Photonics* **7**, 1001–1005 (2013). doi:10.1038/nphoton.2013.274
26. B. Bahari, A. Ndao, F. Vallini, A. El Amili, Y. Fainman, B. Kanté, Nonreciprocal lasing in topological cavities of arbitrary geometries. *Science* **358**, 636–640 (2017). doi:10.1126/science.aao4551 Medline
27. G. Harari, M. A. Bandres, Y. Lumer, M. C. Rechtsman, Y. D. Chong, M. Khajavikhan, D. N. Christodoulides, M. Segev, Topological insulator laser: Theory. *Science* **359**, eaar4003 (2018). doi:10.1126/science.aar4003 Medline
28. M. A. Bandres, S. Wittek, G. Harari, M. Parto, J. Ren, M. Segev, D. N. Christodoulides, M. Khajavikhan, Topological insulator laser: Experiments. *Science* **359**, eaar4005 (2018). doi:10.1126/science.aar4005 Medline
29. N. B. Simpson, K. Dholakia, L. Allen, M. J. Padgett, Mechanical equivalence of spin and orbital angular momentum of light: An optical spanner. *Opt. Lett.* **22**, 52–54 (1997). doi:10.1364/OL.22.000052 Medline
30. M. S. Soskin, V. Gorshkov, M. Vasnetsov, J. Malos, N. Heckenberg, Topological charge and angular momentum of light beams carrying optical vortices. *Phys. Rev. A* **56**, 4064–4075 (1997). doi:10.1103/PhysRevA.56.4064
31. F. Flossmann, U. T. Schwarz, M. Maier, M. R. Dennis, Polarization singularities from unfolding an optical vortex through a birefringent crystal. *Phys. Rev. Lett.* **95**, 253901 (2005). doi:10.1103/PhysRevLett.95.253901 Medline
32. Y. Gorodetski, A. Niv, V. Kleiner, E. Hasman, Observation of the spin-based plasmonic effect in nanoscale structures. *Phys. Rev. Lett.* **101**, 043903 (2008). doi:10.1103/PhysRevLett.101.043903 Medline
33. G. Spektor, D. Kilbane, A. K. Mahro, B. Frank, S. Ristok, L. Gal, P. Kahl, D. Podbiel, S. Mathias, H. Giessen, F.-J. Meyer Zu Heringdorf, M. Orenstein, M. Aeschlimann, Revealing the subfemtosecond dynamics of orbital angular momentum in nanoplasmonic vortices. *Science* **355**, 1187–1191 (2017). doi:10.1126/science.aaj1699 Medline
34. E. Ostrovsky, K. Cohen, S. Tsesses, B. Gjonaj, G. Bartal, Nanoscale control over optical singularities. *Optica* **5**, 283–288 (2018). doi:10.1364/OPTICA.5.000283
35. M. Gilles, P.-Y. Bony, J. Garnier, A. Picozzi, M. Guasoni, J. Fatome, Polarization domain walls in optical fibres as topological bits for data transmission. *Nat. Photonics* **11**, 102–107 (2017). doi:10.1038/nphoton.2016.262 Medline
36. T. Van Mechelen, Z. Jacob, Universal spin-momentum locking of evanescent waves. *Optica* **3**, 118–126 (2016). doi:10.1364/OPTICA.3.000118
37. Available in the materials and methods or supplementary text, as part of the supplementary materials.
38. S. A. Maier, *Plasmonics: Fundamentals and Applications* (Springer, 2007).
39. G. Spektor, A. David, G. Bartal, M. Orenstein, A. Hayat, Spin-patterned plasmonics: Towards optical access to topological-insulator surface states. *Opt. Express* **23**, 32759–32765 (2015). doi:10.1364/OE.23.032759 Medline
40. N. Ocelic, A. Huber, R. Hillenbrand, Pseudoheterodyne detection for background-free near-field spectroscopy. *Appl. Phys. Lett.* **89**, 101124 (2006). doi:10.1063/1.2348781
41. L. Sun, R. X. Cao, B. F. Miao, Z. Feng, B. You, D. Wu, W. Zhang, A. Hu, H. F. Ding, Creating an artificial two-dimensional Skyrmion crystal by nanopatterning. *Phys. Rev. Lett.* **110**, 167201 (2013). doi:10.1103/PhysRevLett.110.167201 Medline
42. D. A. Gilbert, B. B. Maranville, A. L. Balk, B. J. Kirby, P. Fischer, D. T. Pierce, J. Unguris, J. A. Borchers, K. Liu, Realization of ground-state artificial skyrmion lattices at room temperature. *Nat. Commun.* **6**, 8462 (2015).

doi:10.1038/ncomms9462 Medline
43. G. Berruto, I. Madan, Y. Murooka, G. M. Vanacore, E. Pomarico, J. Rajeswari, R. Lamb, P. Huang, A. J. Kruchkov, Y. Togawa, T. LaGrange, D. McGrouther, H. M. Rønnow, F. Carbone, Laser-induced skyrmion writing and erasing in an ultrafast cryo-Lorentz transmission electron microscope. *Phys. Rev. Lett.* **120**, 117201 (2018). doi:10.1103/PhysRevLett.120.117201 Medline
44. T. V. Teperik, A. Archambault, F. Marquier, J. J. Greffet, Huygens-Fresnel principle for surface plasmons. *Opt. Express* **17**, 17483–17490 (2009). doi:10.1364/OE.17.017483 Medline

ACKNOWLEDGMENTS

The Authors would like to thank S. Dolev for his help in fabrication of the measured samples. S.T also acknowledges the generous support of the Jacobs Foundation. **Funding:** This research was supported by "Circle of Light," Israeli Centers for Research Excellence (I-CORE), through the Israel Science Foundation (ISF) grant no. 1802/12; and the European Research Council (Horizon 2020 progarm) grant no. 639172. **Author contributions:** S.T., B.G. and G.B. conceived the project, S.T. and K.C. patterned the samples, E.O., S.T. and K.C. performed the measurements, S.T., N.L. and G.B. performed simulations and analytical calculations. All authors took part in preparing the manuscript. **Competing interests:** The authors declare no competing interests. **Data and materials availability:** All data are available in the main text or the supplementary materials.

SUPPLEMENTARY MATERIALS

www.sciencemag.org/cgi/content/full/science.aau0227/DC1
Materials and Methods
Supplementary Text
Figs. S1 to S5
Reference (*44*)

29 April 2018; accepted 3 July 2018
Published online 19 July 2018
10.1126/science.aau0227

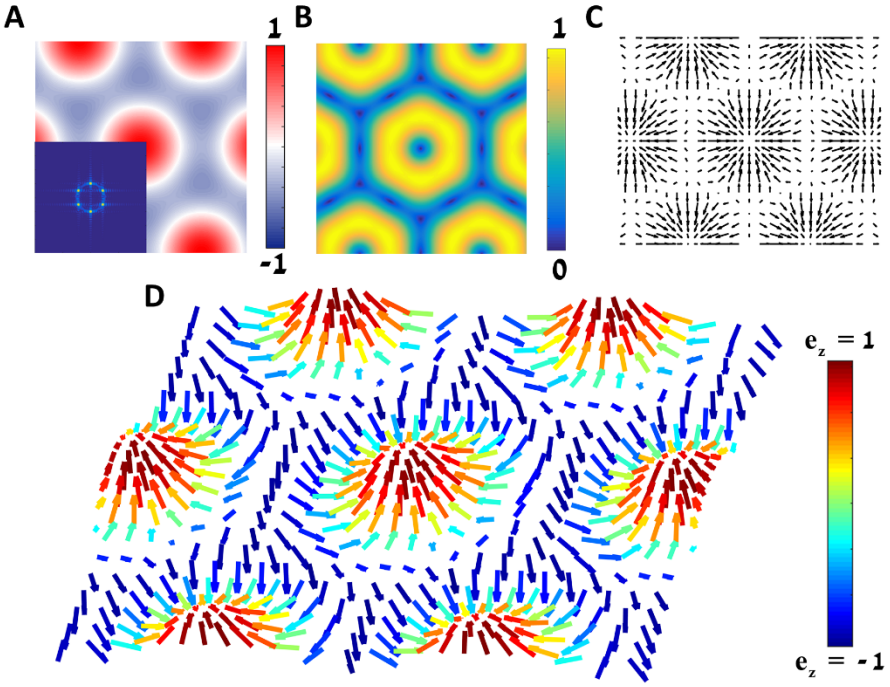

Fig. 1. Calculated electric field distribution of the optical skyrmion lattice. (**A**) Axial (out-of-plane) electric field, according to Eq. 2, with the Fourier decomposition in the inset. (**B**) Amplitude of the transverse (in-plane) electric field (Eq. 3). (**C**) Vector representation of the transverse electric field, showing polarization singularities at the center of each lattice site. (**D**) Vector representation of the local unit vector of the electric field (color coded for the value of its axial component), showing that each lattice site is a Néel-type skyrmion.

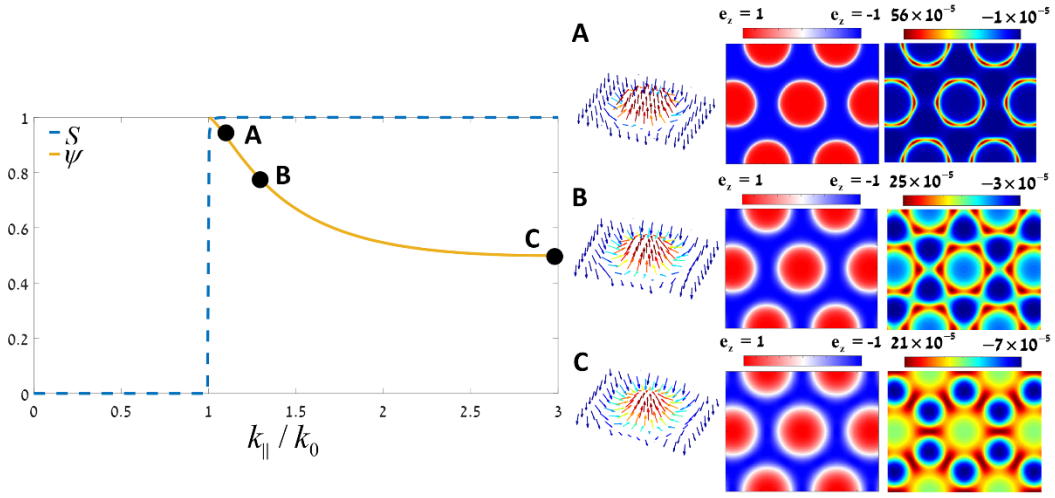

Fig. 2. Tuning of optical topological domain walls, from bubble-type to Néel-type skyrmions. the figure shows the calculated Skyrmion number (blue, dashed) and the skyrmion number density contrast (solid, gold) as a function of the transverse wave vector of the electromagnetic waves. Once the electromagnetic waves gain evanescence in free-space, the skyrmion number jumps to the value of 1, independent of the change in the transverse wave vector. Points A-C have a different skyrmion number density contrast, quantifying the transition from bubble-type to Néel-type skyrmions. Inset are the characteristics of a single lattice site at each of these points, presenting (from left to right): the local unit vector of the electric field (color coded in the same manner as Fig. 1); its axial (out-of-plane) component; and the skyrmion number density. A clear shift from very narrow domain walls separating between two field states (point A), to smeared domain walls (point B) and finally – to virtually non-local domain walls (point C), arises by increasing the transverse wave vector.

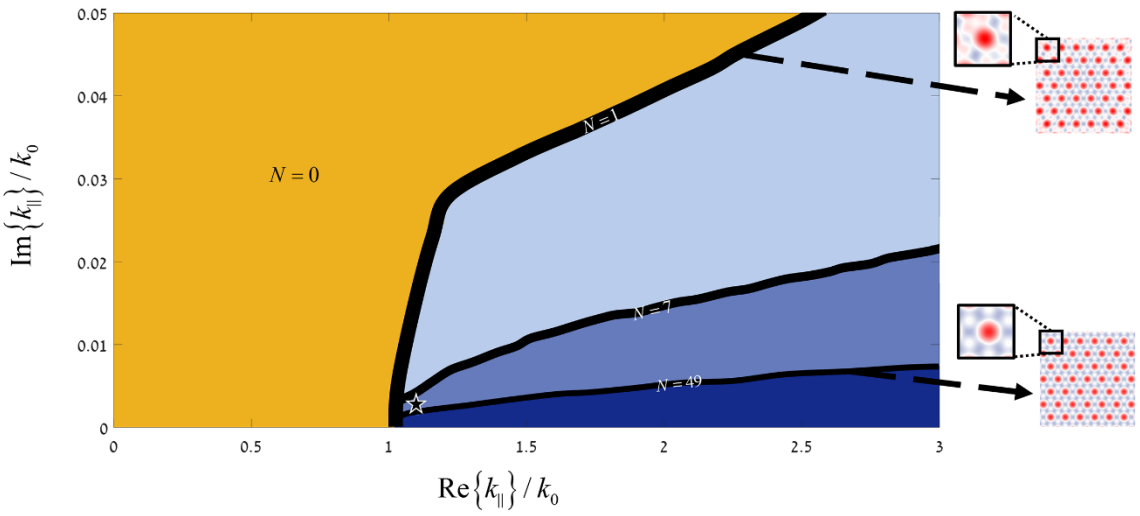

Fig. 3. Theoretical persistence of optical skyrmions in the presence of loss. The figure shows a contour plot of the maximal number of well-defined skyrmions in a lattice (*N*), as a function of the real and imaginary parts of the transverse wave vector. The broad black lines represent the areas where the lattice consists of *N* = 1, 7, 49 well-defined skyrmions. Insets are the amplitude distributions of an *N* = 1 lattice (top right) and an *N* = 49 lattice (bottom right), with a close-up image showing the lattice distortion in non-central sites. Clearly, in the *N* = 1 lattice, only the central lattice site is well-defined. The star represents the experimental conditions of this work (*N* = 37). These results show that by determining the number of well-defined skyrmions in a lattice, it is possible to determine the maximal amount of losses which will destroy its topological invariant. Moreover, they show that even guided modes with a relatively high amount of loss (decaying after 100 oscillations) can create skyrmion lattices.

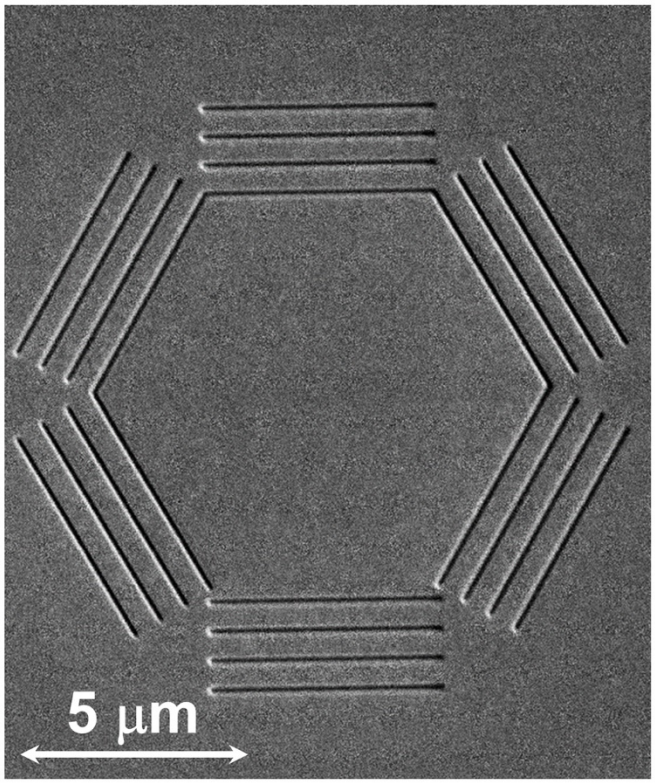

Fig. 4. SEM image of the sample capable of generating an optical skyrmion lattice. The sample consists of six gratings creating a hexagon on a 200 nm Au layer, deposited atop a 1 mm glass substrate. The grating periodicity corresponds to the plasmonic wavelength (636 nm) and the bottom grating is displaced by half the plasmonic wavelength, to enable the necessary phase relations between the interfering waves (a scale bar is available at the bottom-left corner). The optical skyrmion lattice is created at the center of the slit, through the SPPs propagating on the surface of the sample. For more information on the sample, see the materials and methods section in (*40*).

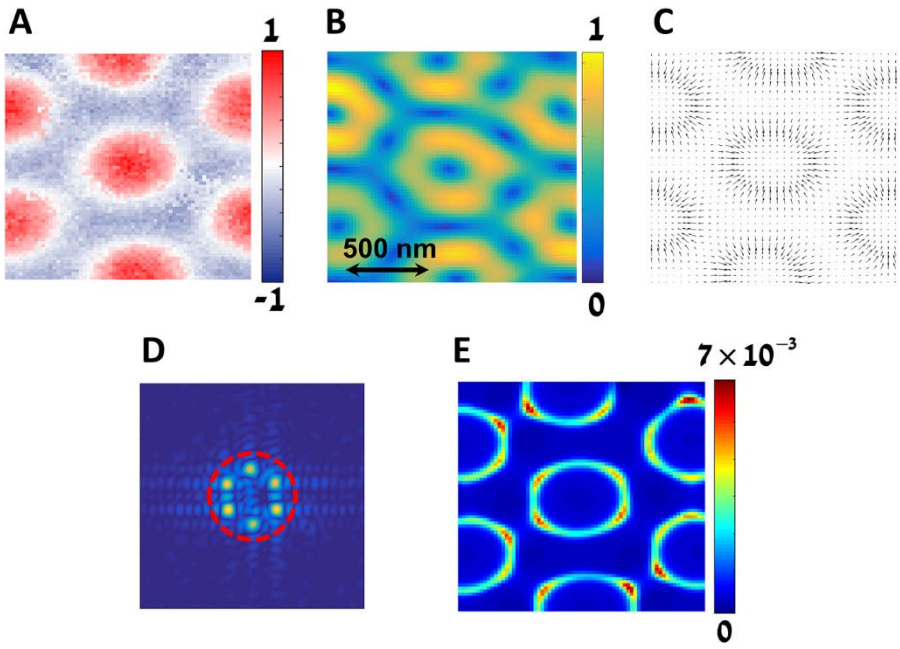

Fig. 5. Measurement of an optical skyrmion lattice created by surface plasmon polaritons. (**A**) Real part of the axial (out-of-plane) electric field at the center of the sample described in Fig. 3 (without noise-filtering). (**B**) Amplitude of the transverse (in-plane) electric field. (**C**) Vector representation of the transverse electric field. (**D**) Amplitude of the Fourier decomposition of the longitudinal electric field. (**E**) Skyrmion number density map of the lattice. Scale bar is inset (B). The complex value of the axial electric field was measured with 20 nm resolution by the system described in Fig. 3, and measurement noise was filtered with the low-pass filter appearing in (D) as a red (dashed) circle. (B), (C), and (E) were then extracted from the data. The measured skyrmion number of a single lattice site was $S = 0.997 \pm 0.058$, which, together with the figures, shows a good match to the theoretical prediction. Actual number of lattice sites in our sample was 37.

Optical skyrmion lattice in evanescent electromagnetic fields

S. Tsesses, E. Ostrovsky, K. Cohen, B. Gjonaj, N. Lindner and G. Bartal

published online July 19, 2018